Multiphoton single and double ionization of neon in the EUV

OPEN ACCESS
IOP Publishing
Journal of Physics B: Atomic, Molecular and Optical Physics
J. Phys. B: At. Mol. Opt. Phys. **58** (2025) 015601 (9pp)
https://doi.org/10.1088/1361-6455/ad4078

Multiphoton single and double ionization of neon in the EUV

Stephen M Durkan[1,2,*], Vincent Richardson[1,*], Andrew Forembski[1], Lazaros Varvarezos[1,2], Denis Cubaynes[3,4], Stefan Düsterer[5], Pavle Juranić[6], Wenbin Li[7], Mathias Richter[8], Kai Tiedtke[5], Michael Meyer[9], L A A Nikolopoulos[1] and John T Costello[1,2]

[1] School of Physical Sciences, Dublin City University, Dublin, Ireland
[2] National Centre for Plasma Science and Technology, Dublin City University, Dublin, Ireland
[3] Université Paris Saclay, CNRS, Institut des Sciences Moléculaires d'Orsay, Orsay F-91405, France
[4] Synchrotron SOLEIL, L'Orme des Merisiers, Gif Sur Yvette, BP 48, F-91192, France
[5] DESY, D-22607 Hamburg, Germany
[6] Paul Scherrer Institut, Forschungsstrasse 111, 5232 Villigen PSI, Switzerland
[7] Tongji Univ, School of Physics Science and Engineering, Key Laboratory of Advanced Micro-Structured Materials—MOE, Shanghai, People's Republic of China
[8] Physikalisch-Technische Bundesanstalt, D-10587 Berlin, Germany
[9] European XFEL, Holzkoppel 4, D-22869 Schenefeld, Germany

E-mail: stephen.durkan3@mail.dcu.ie and richarv2@gmail.com

Received 19 December 2023, revised 27 March 2024
Accepted for publication 18 April 2024
Published 5 December 2024

Abstract

New information demonstrating the importance of both sequential and simultaneous (or direct) multiphoton ionization of inner shell electrons from neon is discussed in this paper. Ne was irradiated with intense 93 eV free electron laser (FEL) pulses at FLASH and studied with the aid of photoelectron spectrometry. This resulted in two and three photon, single and double ionization of neon, removing electrons from 2s and 2p subshells of the neutral Ne atom in multiple different pathways. The spectral features of the photoelectrons were identified through comparison with the NIST database and field averaged time-dependent density matrix theory. The calculations show the direct multiphoton ionization processes to be extremely sensitive to the focused FEL intensity.

Keywords: multiphoton ionisation, free electron laser, photoelectron spectroscopy

1. Introduction

Atomic photoionization has been an active field for spectroscopic investigations since the first observation of the photoelectric effect by Hertz in 1887 [1] and the subsequent explanation by Einstein in 1905 [2]. In that case, it was observed that in order to liberate an electron, the energy of the incoming photon was simply required to be greater than the work function of the material under investigation. Subsequently, the pioneering theoretical work of Göppert-Mayer [3] showed that a two-photon absorption process was also possible, resulting in photoionization provided that the sum of the photon energies exceeded the ionization threshold. However, for a two-photon process to occur, the brightness of the light source should be sufficiently high.

Inner-shell and core level atomic, single-photon ionization has been exhaustively studied at synchrotron facilities, over the last several decades for atoms, molecules and their corresponding ions [4–9]. Over the course of time, technological progress resulted in the development of so-called free electron

* Authors to whom any correspondence should be addressed.

lasers (FELs) [10–16]. In contrast to the third-generation synchrotrons [17], FELs exhibit high enough brightness to induce nonlinear processes such as multi-photon ionization in the Extreme-UV (EUV) and x-ray photon energy region [18], thus setting a landmark. The very nature of these experiments is fundamental, thereby providing information regarding the electronic structure in atoms and molecules. As x-ray FELs start to produce pulses down to the attosecond timescale [19] it becomes possible to follow the process on inherent atomic timescales (e.g. [20]). In addition, a deep understanding of photoionization can also pave the way to unveiling the mechanisms underlying interaction of light with more complex molecular systems (e.g. [21–23]).

Early experiments on nonlinear photoionization processes were performed at the FLASH FEL in Hamburg where Wabnitz *et al* [24] observed the sequential multiphoton ionization of Xe and Ar irradiated by FEL pulses tuned to a wavelength of 98 nm. Similarly, Sorokin *et al* [25] studied direct, sequential and resonant N-photon ionizations of Ne, using photon energies of 38.4 and 42.8 eV ($N = 2$–4). The Heidelberg reaction microscope (REMI) was used by Moshammer *et al* [26] to investigate the nonsequential ionization of Ne and Ar, irradiated by photons at 39 eV, delivered by the FLASH FEL. The ionization of Xe in the region of the *4d-εf* giant resonance using photons at 93 eV, was examined at the same FEL facility, resulting in a high degree of ionization up to a charge state of Xe^{21+} [27]. This finding was further confirmed by a subsequent study, where ionization of Kr, Xe, Ne and Ar was induced by FEL photons also tuned to an energy of 93 eV. In this case a significantly higher degree of ionization was observed for Xenon compared to the other rare gases [28]. In all these campaigns the so-called ion time-of-flight (TOF) technique was applied to record the yields of the ion products. Ion TOF measurements were also performed at other FEL facilities including LCLS [29] using a higher photon energy (ca. 1100 eV) and SCSS using a lower photon energy (ca. 20 eV) [30]. Recently a sequential three vacuum-UV photon absorption process has been invoked to explain the results of an experiment on charge transfer in argon dimers [31].

In order to complement the ion measurements, experiments involving photoelectron spectroscopy have been performed. Photoelectrons, carry valuable information associated on the electronic structure of atoms and molecules. For example electron spectroscopy has been used to make observations of direct two photon ionization of atoms [32, 33] while theoretical efforts on such direct two photon EUV processes continue [34]. Double core holes leading to 'hollow ions' with empty 1s subshells are another example of the product of non-linear interactions of intense and short x-ray FEL pulses with atoms and molecules [35–37]. Some experiments have combined ion and electron spectroscopy to track the respective roles of photo- and Auger–Meitner ionization processes as they led to very high charges states in atoms exposed to intense x-ray FEL fields [38]. In addition, angle resolved measurements have been reported in the literature [39–41], with one such experiment particularly relevant here as it reported both two photon double ionization and three photon triple ionization [42]. What differentiates it from our work is that both pathways were exclusively sequential with electrons produced at correspondingly much lower kinetic energies than here.

Experiments on atoms exposed to intense bichromatic fields, where focused FEL pulses have been used in combination with near infrared laser fields to investigate two-colour ionization, have also been reported [32, 43, 44]. Further details of developments and work at EUV and x-ray FELs can be found in many review articles and special issues [18, 45–53]. In the interests of completeness, we note also that two EUV photon double ionization of Ne using a high brightness high harmonic light source has been reported in the literature [54].

We report here some archival electron spectroscopic measurements on Ne irradiated by tightly focused FLASH FEL pulses tuned to a photon energy of 93 eV, recorded during a campaign on Xe photoionization [33]. The relook at the Ne data, and new efforts to elucidate it theoretically, are motivated by the high peak intensity afforded by the very short pulses (ca. 20 fs) and tight focus (ca. 3 μm) available at that time. By comparing the results of field averaged time-dependent density matrix theory [55] with the experimental results it was possible to identify a number of pathways leading to two-photon single and three-photon double ionization of neon.

2. Materials and methods

2.1. Experiment

This experiment was performed at the BL3 beamline of the FLASH (now designated FLASH1) FEL [11]. The experimental setup is described in [33], thus only a brief description is given here. The FEL was operated in single-bunch mode at a repetition rate of 5 Hz and at a central photon energy of 93 $\pm$1 eV. The FEL pulse energy varied between 10 μJ and 45 μJ and was monitored by means of the Gas Monitor Detector (GMD) to track any shot-to-shot fluctuations [56]. The FEL beam was focused down to a spot of diameter 3 μm using a spherical Mo/Si multilayer mirror [57] with a reflectance of around 65%. The peak intensity at the focus was of the order of 10^{16} W cm^{-2} allowing for observation of multi-photon ionization, both direct and sequential. The base pressure was 2×10^{-8} mbar and the operating pressure during the measurements was 1×10^{-6} mbar.

Photoelectron spectra were acquired using a magnetic bottle electron spectrometer [58, 59] installed at BL3. The optimum achievable energy resolution of the spectrometer was estimated to be around 5% of the measured kinetic energy. In order to discriminate against the low kinetic energy photoelectrons, a retardation voltage was applied to the entrance aperture to the TOF. The photoelectron signal due to the unfocused FEL beam (several mm diameter) was observed by placing a beam block in front of the mirror. By doing so, it was also possible to take into account the weak contributions of the second harmonic of the FEL beam. Furthermore, background signals (i.e. in the absence of Ne gas) were recorded and subtracted from the experimental spectra. Each spectrum presented in this work corresponds to an average of 100 single-shot spectra to minimize the effect of pulse-to-pulse fluctuations. The

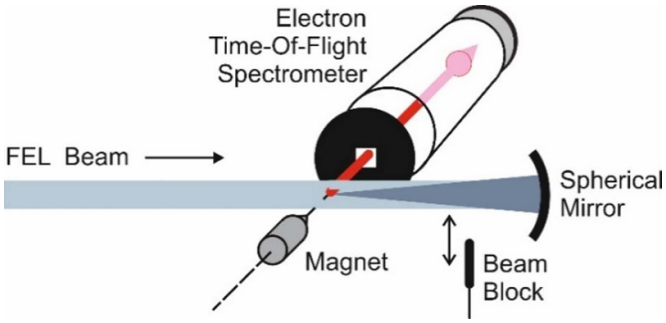

Figure 1. Experimental setup: a magnetic bottle type electron spectrometer was used to record electron kinetic energy distributions. Focusing of the 93 eV FEL beam was achieved by means of a spherical Mo-Si multilayer mirror. Spectra were taken with both unfocused, and focused FEL beams. Unfocused beams were made available in the chamber by inserting a beam block into the beam, between the TOF and the spherical mirror [33, 60]. Reprinted figure with permission from [33], Copyright (2010) by the American Physical Society.

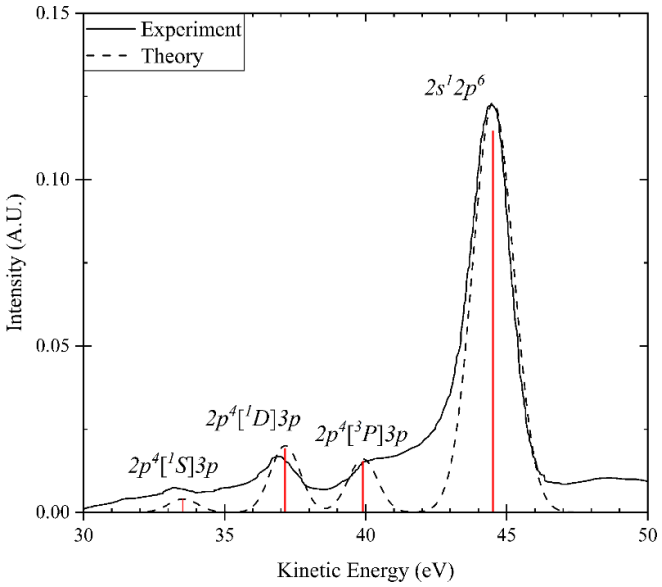

Figure 2. Electron energy spectrum produced by the interaction of Ne gas with an unfocused FLASH beam tuned to a photon energy of 93 eV (intensity $\sim 10^{10}$ W cm^{-2}, smooth curve). Red sticks represent the calculated transitions, and the dashed curve shows a convolution of Gaussian profiles with the theoretical calculations, representing the linewidth of the FEL beam and the spectrometer resolution. Labels indicate the post-ionisation electron configuration of the Ne^+ ions [60].

TOF traces were recorded with the aid of a fast digital oscilloscope (LeCroy Wavemaster 8600A). A schematic diagram of the experimental setup is shown in figure 1.

Figure 2 shows the photoelectron spectrum in the 30–50 eV region corresponding to the average of the 100 single-shot spectra at the lowest FEL intensity, obtained with the beam block in place. Additionally, the calibration of the microchannel plate (MCP) is ensured by the energies and relative intensities of the visible peaks which agree with previously reported synchrotron experiments [61, 62].

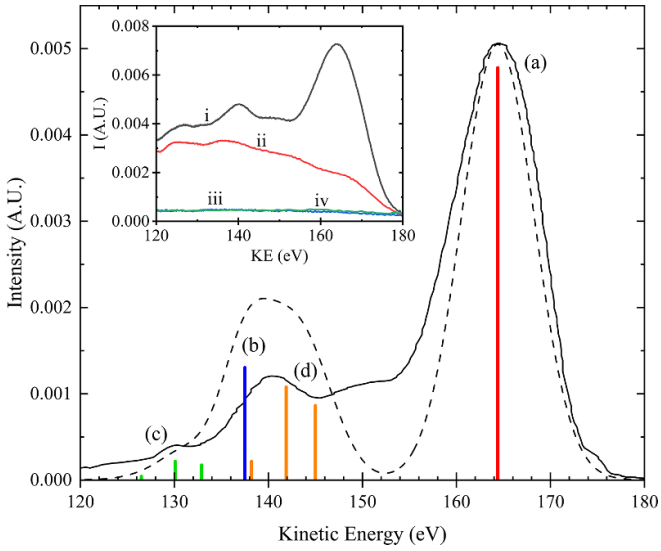

Figure 3. Electron energy spectrum produced by the multiphoton interaction of Ne with a 93 eV FEL field, using the focused beam (of the order of 10^{16} W cm^{-2}) at FLASH (smooth curve). The peak labels (a)–(d) are explained in the main text. The sticks represent the calculated transitions and are coloured to match the pathways depicted in figure 4. The theoretical curve (dashed line) is formed by convolving the transitions with two Gaussian curves representing the FEL linewidth and the spectrometer resolution. The inset figure shows the signal from the focused FEL beam in Ne (black, i), the focused beam in residual gases (red, ii), the unfocused beam in Ne (blue, iii) and the unfocused beam in residual gases (green, iv). The lack of structure in trace (iii) indicates that the second harmonic contributes little to the overall signal.

Figure 3 shows the experimental spectrum in the 120–175 eV photon energy region, obtained for a higher FEL intensity on the order of 10^{16} W cm^{-2} (focused FEL beam). In this case a -90 V retarding field was applied to the MBES entrance aperture in order to reject low-energy photoelectrons associated with single-photon ionization of Ne. Hence, the spectrum is dominated by features originating from two-photon double ionization of the neutral atom and the singly charged ion, as will be explained later. The widths of the spectral features are determined by a combination of FEL bandwidth and the resolution of the electron spectrometer. Accounting for the -90 V retardation voltage and assuming that the broadening due to the MBES is representable by a Gaussian profile, the $2p^{-1}$ line experiences an instrumental broadening of ca. 3.5 eV while the value for the $2s^{-1}$ line in the vicinity of 140 eV is closer to 2.5 eV. The effect of the additional 1 eV due to the FEL bandwidth on the lines is quite small (post convolving the two Gaussian functions) but is nevertheless included for these features.

2.2. Time-dependent density matrix equations in the FEL field

We simulate the photoionization processes via a density matrix formalism which facilitates the elimination of non-essential states leading to a reduced set of equations of motion (EOMs) for the dynamics of the neon ground

state $|\mathrm{Ne};0\rangle$, and the continua of interest associated with the singly-ionised neon states $|\mathrm{Ne}^+;i\rangle$, $i=1-5$ ($\mathrm{Ne}^+(1s^22s^22p^5)$, $\mathrm{Ne}^+(1s^22s^12p^6)$, $\mathrm{Ne}^+(1s^22s^22p^4[^3P]3p)$, $\mathrm{Ne}^+(1s^22s^22p^4[^1D]3p)$, $\mathrm{Ne}^+(1s^22s^22p^4[^1S]3p)$) as well as the three doubly ionised states, $|\mathrm{Ne}^{2+};i\rangle$, $i=6$–8 ($\mathrm{Ne}^{2+}(1s^22s^22p^4[^3P]$, $(1s^22s^22p^4[^1D])$, $(1s^22s^22p^4[^1S])$. The former $i=1-5$ continua are reached via two-photon absorption processes from the Neon ground state while the $i=6-8$ continua are accessed via a three-photon sequential double ionisation process, namely one photon from Ne to Ne^+ and two-photons from Ne^+ to Ne^{2+} ($|\mathrm{Ne};0\rangle+\omega\rightarrow|\mathrm{Ne}^+;1\rangle+2\omega\rightarrow|\mathrm{Ne}^{2+};i\rangle$, $i=6-8$). In the present case of $\omega=93$ eV, the dominant channel is one-photon absorption, the dynamics of which is governed by the corresponding total ionisation widths $\gamma_a^{(1)}$, where $a=\mathrm{Ne},\ \mathrm{Ne}^+$. On the other hand, the simulated photoelectron spectrum, is dominated by two-photon absorption processes from the Ne and Ne^+ ground states and is accordingly represented by the corresponding partial ionisation widths $\gamma_{a;i}^{(2)}$, where i represents the corresponding continuum channel.

Given the above clarifications, and following a standard procedure within a time-dependent perturbative approach, the EOMs for the neon density matrix elements are derived starting off with the Liouville equation [63]. Within this procedure a rotating-wave-approximation (RWA) takes place which leads to a set of EOMs parametrised in terms of slowly varying matrix elements and ionisation widths connecting to the respective continua.

Further to this, the solution of the EOMs considers that the FEL radiation field is a partially coherent field, i.e. it exhibits amplitude and phase fluctuations. In this case, the FEL radiation field $\mathcal{E}(t)$ is modelled via its coherence functions. Here we take $\langle\mathcal{E}(t)\rangle=0$, while for the field's and intensity's first order coherence functions we have assumed:

$$\langle\mathcal{E}(t)\,\mathcal{E}^*(t')\rangle=\mathcal{E}_0^2\,e^{-\frac{\chi t^2+\chi^* t'^2}{2\tau_p^2}}\,e^{-\frac{(t-t')^2}{2\,\tau_c^2}}$$

where the brackets represent ensemble averages of the FEL radiation; τ_p characterises the duration of the averaged time-profile of the intensity, $\chi=1-i/\sqrt{3}$; τ_c is the field's characteristic coherence time. From the above equations, the mean field intensity is given by $\langle I(t)\rangle=\mathcal{E}_0^2 e^{-\frac{t^2}{\tau_p^2}}$ and $\langle I^2(t)\rangle=2\langle I(t)\rangle^2$. A field with these properties (satisfying Gaussian statistics), regarded as a sufficiently good model, has been studied from the viewpoint of a shot-noise random field resulting in a random intensity with an exponential probability distribution law and a Gamma-like distribution of its fluctuating energy, close to the characteristic of an actual FEL field [55]. The main parameters which characterise the fluctuations are their strength ($\mathcal{E}_0$) and coherence time (τ_c). The latter time effectively defines an extra characteristic dynamic time scale. We considered these fluctuations by (ensemble) averaging the EOMs of the density matrix elements over the FEL pulses leading to the following set of equations:

$$\frac{\mathrm{d}}{\mathrm{d}t}\langle\sigma_{\mathrm{Ne}}(t)\rangle=-\left(\gamma_{\mathrm{Ne}}^{(1)}\langle I\rangle+\gamma_{\mathrm{Ne}}^{(2)}\langle I^2\rangle\right)\langle\sigma_{\mathrm{Ne}}(t)\rangle,$$

$$\frac{\mathrm{d}}{\mathrm{d}t}\langle\sigma_{\mathrm{Ne}^+}(t)\rangle=-\left(\gamma_{\mathrm{Ne}^+}^{(1)}\langle I\rangle+\gamma_{\mathrm{Ne}^+}^{(2)}\langle I^2\rangle\right)\langle\sigma_{\mathrm{Ne}^+}(t)\rangle+\frac{\mathrm{d}}{\mathrm{d}t}\langle\sigma_{\mathrm{Ne}}(t)\rangle.$$

The above set of equations describe the evolution of the Ne and Ne^+ ensemble-averaged populations (represented by $\langle\sigma_{\mathrm{Ne}}\rangle$ and $\langle\sigma_{\mathrm{Ne}^+}\rangle$, respectively) by taking into account only the total one- and two-photon absorption processes via the corresponding total ionisation widths. On the other hand, the photoelectron spectrum for the energy range of interest is dependent on the population of the neon species and on the partial ionisation widths as seen from the following equation:

$$\begin{aligned}\frac{\mathrm{d}}{\mathrm{d}t}&\langle\sigma_{\epsilon\epsilon}(t)\rangle\\&=\sum_{i=1}^{5}\gamma_{\mathrm{Ne}^+}^{(2)}\frac{\left|\mathrm{d}_{\mathrm{Ne};i}^{(2)}\right|^2}{\left[\epsilon-(E_0+2\omega-E_i)\right]^2+\left(\frac{\gamma_{\mathrm{Ne};i}^{(2)}}{2}\right)^2}\left\langle I^2\right\rangle\langle\sigma_{\mathrm{Ne}}(t)\rangle\\&\quad+\sum_{i=6}^{8}\gamma_{\mathrm{Ne}^+}^{(2)}\frac{\left|\mathrm{d}_{\mathrm{Ne}^+;i}^{(2)}\right|^2}{\left[\epsilon-(E_1+2\omega-E_i)\right]^2+\left(\frac{\gamma_{\mathrm{Ne}^+;i}^{(2)}}{2}\right)^2}\left\langle I^2\right\rangle\langle\sigma_{\mathrm{Ne}^+}(t)\rangle.\end{aligned}$$

In the above $\langle\sigma_{\epsilon\epsilon}(t)\rangle$ represents the ensemble-averaged population dynamics of the continuum states, generated by two-photon absorption from the Ne (first term) and Ne^+ (second term) ground states. E_i represents the energies of the neon ionisation species involved in the calculation.

The pulse duration (τ_{ph}) can be evaluated from the expression, $\tau_{\mathrm{ph}}=0.7\times M\times\tau_{\mathrm{c}}$, where M is the number of modes and $\tau_{\mathrm{c}}$is the coherence time [64]. We can estimate the number of modes present in the beam from $M\approx1.4\times N_{\mathrm{spect}}$, where $N_{\mathrm{spect}}\approx5$ is the mean number of spikes present in the SASE FEL spectrum [64]. For the operational mode of FLASH at the time of the experiment the coherence time was determined by the measurement of the field gain length to be about 4 fs [11], which is in good agreement with FEL beam dynamics simulations using the FAST code [65]. Thus, a pulse duration of $0.7\times M\times\tau_c\approx20$ fs was deduced for the present case. This, along with the fact that non-resonant ionisation takes place with the 93 eV pulse, suggests that the experimental data can be described with sufficient accuracy based on the averaged intensity moments $\langle I^n(t)\rangle$, $n=1,2$ and the one and two photon ionisation widths γ_{ni}. The latter requires for the validity of the averaged EOMs that the field intensity should not reach ionisation saturation conditions within the time scale of the *coherence time*.

The EOMs were solved using a pulse of peak intensity of 8×10^{15} W cm^{-2} and mean pulse duration of 20 fs.

We have also considered a volume integration of the signal to take into account the one-photon saturation of the ionization yield. The field was modelled to radially

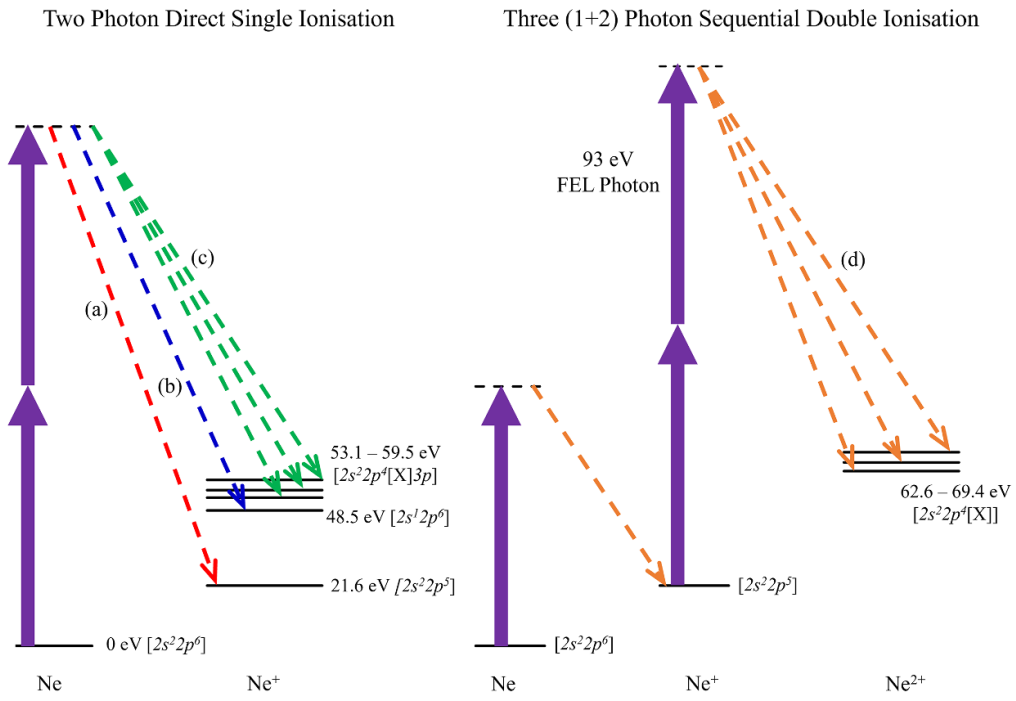

Figure 4. Partial Grotian diagram indicating the different ionization pathways responsible for the spectral features labelled in figure 4: (a) red, two photon ionization of a *2p* electron from neutral Ne; (b) blue, two photon ionization of a *2s* electron from neutral Ne; (c) green, two photon ionization of a *2p* electron from ground state Ne leaving the Ne^+ ion in a manifold of excited satellite (shake up) states; (d) orange, one photon ionization of Ne followed by two photon ionization of a 2p electron from the ground state Ne^+, resulting in $2s^2 2p^4$[X] states of Ne^{2+} where X = ^3P, ^1D, ^1S. X corresponds to the same terms in case (c).

Table 1. LS-coupling is assumed for the spectroscopic designation of the states; also $n_i = E_0 + 2\omega - E_i$, $i = 1-5$ and $n_i = E_1 + 2\omega - E_i$, $i = 6-8$. Each state is labelled as the path it contributes to in the multi-photon spectrum (figure 4). The two-photon cross sections have been calculated based on a scaling approach and a simple consideration of the ratios of the grand-parentage configuration scheme.

i	State	^{2S+1}L	E_i (eV)	ϵ_{1i} (eV)	ϵ_{2i} (eV)	$\sigma^{(1)}_{\mathrm{Ne};i}$ (Mb)	$\sigma^{(2)}_{\mathrm{Ne};i}$ $(\times 10^{-52}$ cm^4 s$)$	$\sigma^{(2)}_{\mathrm{Ne}^+;i}$ $(\times 10^{-52}$ cm^4 s$)$	Path
0	$2s^2 2p^6$	^1S	0	—	—	—	—	—	—
1	$2s^2 2p^5$	^2P	21.6	71.4	164.4	3.1	1.36	—	a
2	$2s 2p^6$	^2S	48.48	44.2	137.52	0.87	0.272	—	b
3	$2s^2 2p^4$ [^3P] $3p$	^2P	53.1	39.9	132.9	0.12	0.048	—	c_1
4	$2s^2 2p^4$ [^1D] $3p$	^2P	55.85	37.15	130.15	0.15	0.045	—	c_2
5	$2s^2 2p^4$ [^1S] $3p$	^2P	59.47	33.53	126.53	0.028	0.009	—	c_3
6	$2s^2 2p^4$	^3P	62.6	52	145	—	—	0.045	d_1
7	$2s^2 2p^4$	^1D	65.7	48.9	141.9	—	—	0.056	d_2
8	$2s^2 2p^4$	^1S	69.44	45.16	138.16	—	—	0.013	d_3

decay as a Gaussian away from its centre and we have ignored any spatial variations along the FELs propagation axis.

In figure 4 we show the partial energy diagram that allows for identification of the spectral features, present in the FEL electron spectrum at high kinetic energies (corresponding to two and three photon processes). This energy diagram was constructed using the energy levels for Ne and Ne^+ tabulated in the NIST database [66]. The electron spectrum resulting from one photon absorption is shown in figure 2, where features due to *2s*-subshell ionization and $2p^4 nl$ satellite states are labelled. The electron spectrum resulting from multi-photon ionization is shown in figure 3 where the coloured bars correspond to computed transitions shown as coloured arrows in figure 4.

The states of Neon included in the theoretical calculations are those indicated in figure 4 and listed in table 1, along with the values for the one- and two-photon cross sections for the individual pathways from the Ne and Ne^+ ground states. The relationship between the ionisation widths and the corresponding generalised cross sections is $\gamma^{(N)}_{a;i} = \sigma^{(N)}_{a;i}\left(\frac{I}{\hbar\omega}\right)^N$, $N = 1,2$ in SI units.

The $\sigma^{(1)}_{\mathrm{Ne}}$ and $\sigma^{(1)}_{\mathrm{Ne};1}$ values used were taken from the experimental measurements [24, 26]. For the $\sigma^{(2)}_{\mathrm{Ne}}$ estimation a scaling approach was followed as described in [67]. Finally for the partial ionisation cross sections to $i = 3-5$ and $i = 6-8$,

the ratios based on the grand parentage configurations for the ^3P, ^1D, ^1S are also in approximate agreement with the experimental data reported in [60].

3. Discussion

It is observed that the spectrum presented in figure 2 is dominated by features associated with the process of single photon ionization of Ne. This spectrum is used as a benchmark for the energy calibration of the spectrometer. The features observed in this region are identified as follows: the peak around 44 eV is due to $2s^{-1}$ ($2s^1 2p^6\,^2S$) photoionization of the neutral atom and the features in the region below 40 eV are due to the $2p^4nl$ satellites in Ne^+. Specifically, the $2p^4 3p[^3P]\,^2P$ peak is discernible within the resolution of the experiment whereas the other satellites could not be resolved. However, these peaks have been observed and reported in the literature [62].

The observed spectral width of the $2s^{-1}$ feature just below 45 eV in figure 2 can be predominantly attributed to a combination of the spectral bandwidth of the FEL (approx. 1 eV) with the resolution of the magnetic bottle electron spectrometer (ca. 5% of the pass energy). Here a retardation voltage of 20 volts was applied and so the pass energy was reduced by the corresponding amount. The natural linewidth, calculated as approximately 0.15 eV, is much narrower and so is dominated by the experimental widths. Likewise in the case of the satellite lines, their natural widths were convolved with the MBES instrument function and FEL bandwidth which results in the broad and unresolved features observed at lower kinetic energies in the figure. Overall, the theoretical main and satellite line positions and thus the overall predicted electron spectrum is in very good agreement with the experimental data.

The broad feature centred on 164 eV in figure 3 is associated with the direct two-photon ionisation of a $2p$ electron from the neutral atom. This channel results in a photoelectron with energy of:

$$2 \times (93 \pm 1) - 21.6 = 164 \pm 2 \text{ eV}$$

in agreement with the observed position of the peak (a) and supported by the calculations.

The peak labelled as (b) in figure 3 (blue transition) results from the direct two-photon ionisation of a $2s$ electron from neutral neon. The expected energy for this photoelectron channel is:

$$2 \times (93 \pm 1) - 48.48 = 138 \pm 2 \text{ eV}$$

in agreement with the position of the peak (b) observed in figure 3 and supported by the calculations. Thus both peaks can be easily identified due to their close agreement with the theoretically calculated energies.

The weak feature (labelled as (c), green transitions) is due to $2s^2 2p^4 nl$ satellite states in Ne^+, specifically the $2p^4 3p$ states that were also observed in the single photon case, as shown in figure 2. The calculations result in similar intensities in this region. As satellite peaks, they have much smaller probabilities than the $2s^{-1}$ photoelectron line.

The remaining peak (d) is attributed to sequential one photon ionization of neutral Ne with two photon double ionisation of Ne^+. There are multiple thresholds which can be easily accessed, that result in further ionization of Ne^+ via a two-photon process in the second step [66]. These energy thresholds and the corresponding electron configurations are listed in table 1 ($i = 6 - 8$). Two-photon ionization of singly charged Ne leaving doubly charged neon in these states yields a series of lines with kinetic energies ranging between 138 and 145 eV. This range corresponds with structure (d) and the orange transitions in figure 3, suggesting it is at least partly due to electrons emitted by sequential three-photon double ionisation of neon, where the first photon leaves Ne^+ in its ground electronic state.

The theoretical and calculated spectra agree quite closely, in particular for the strong 1-photon $2s^{-1}$ and $2p^{-1}$ peaks that are well reproduced in both electron energy and transition intensity. The discrepancies between the experimental and calculated spectra in the 2-photon spectrum may be attributed to the stochastic features and strength of the FEL radiation as well as the approximate values used for the cross-sections [68]. For example, the uncertainty regarding the number of FEL modes that contribute to the observed spectrum would lead to differing probabilities. Moreover, the high peak value of the intensity saturates the first step of the ionization process which in turn makes the calculation of the two-photon ionization peaks, originating from the singly ionized neon, very sensitive to the exact value of the intensity.

Alternative pathways to produce these spectra from the ones described above can be ruled out by semi-quantitative analysis and previously identified energy levels. Specifically, two photon ionisation of a $2s$ electron from Ne^+ would result in photoelectrons with kinetic energy less than 120 eV, due to the binding energy of approximately 66.2 eV in this case [66]. Therefore, this pathway cannot be responsible for features in the spectrum shown in figure 4. Similarly, photoelectrons emitted from $2s$ and $2p$ subshells of Ne^{2+} or higher charge states would also have kinetic energies below 120 eV.

In pathway (d), the Ne^+ intermediate is produced upon single photon absorption from neutral neon in the first step. Theoretically, the two-photon pathway (a) could also be responsible for this first step, but the probabilities of these ions interacting with two additional photons is very low and can be ignored. K-shell electrons can obviously be ignored, as their high binding energies would require at least 10 photons to eject an electron from even the neutral neon [69], a scale far beyond the realistic reach of the intensities used in this experiment. Thus, the pathways (a)–(d) described previously are the only plausible explanation for the observed spectrum.

The modulation in the figure 3 around 150 eV along with the asymmetric profile of the $2p^{-1}$ line manifest on its low energy side are indicators of unresolved structure between features labelled (a) and (d). At this point we do not have

plausible designations for these features and so we must leave this region unassigned for now.

4. Conclusions

Two photon single ionization and 1 + 2 (three photon) double ionization of Ne has been observed in an experiment at the FLASH FEL where intense pulses, tuned to a photon energy of 93 eV, were used to irradiate a low density atomic beam. Spectral signatures of four different photoionization channels have been observed in the photoelectron spectra. These channels have been identified with the aid of data available in the NIST database and theoretical calculations. The calculations show that the multiphoton spectra are very sensitive to FEL intensity and are measurable when the irradiance approaches values close to 10^{16} W cm^{-2}. Structure in the electron spectrum in the kinetic energy region around 150 eV cannot, as yet, be plausibly assigned.

Data availability statement

The data cannot be made publicly available upon publication because the cost of preparing, depositing and hosting the data would be prohibitive within the terms of this research project. The data that support the findings of this study are available upon reasonable request from the authors.

Acknowledgments

S M D, L V and J T C acknowledge support from Science Foundation Ireland Grant No. 19/FFP/6956. Work associated with EU COST Action No. CA17126 (TUMIEE). A F would like to acknowledge the financial support of the Irish Research Council (IRC) under the postgraduate research funding scheme, Funding Code: GOIPG/2018/1070. M M acknowledges support from the Deutsche Forschungsgemeinschaft (DFG, German Research Foundation), SFB-925, Project 170620586. We are deeply grateful to Josef Feldhaus (Ret'd) and Andrey Sorokin (RIP) for their contributions to this work. We acknowledge DESY (Hamburg, Germany), a member of the Helmholtz Association HGF, for the provision of experimental facilities.

ORCID iDs

Stephen M Durkan https://orcid.org/0000-0001-6489-0389
Lazaros Varvarezos https://orcid.org/0000-0002-6781-6616
Stefan Düsterer https://orcid.org/0000-0003-4379-1327
L A A Nikolopoulos https://orcid.org/0000-0002-5996-5400
John T Costello https://orcid.org/0000-0003-4677-9999

References

[1] Hertz H 1887 Ueber Einen Einfluss Des Ultravioletten Lichtes Auf Die Electrische Entladung *Ann. Phys.* **267** 983–1000
[2] Einstein A 1905 Über Einen Die Erzeugung Und Verwandlung Des Lichtes Betreffenden Heuristischen Gesichtspunkt *Ann. Phys.* **322** 132–48
[3] Göppert M 1929 Über Die Wahrscheinlichkeit Des Zusammenwirkens Zweier Lichtquanten in Einem Elementarakt *Naturwissenschaften* **17** 932
[4] Madden R P and Codling K 1963 New autoionizing atomic energy levels in He, Ne, and Ar *Phys. Rev. Lett.* **10** 516–8
[5] Ueda K 2003 High-resolution inner-shell spectroscopies of free atoms and molecules soft-x-ray beamlines at the third-generation synchrotron radiation *J. Phys. B: At. Mol. Opt.* **36** R1–R47
[6] West J B 2001 Photoionization of atomic ions *J. Phys. B: At. Mol. Opt.* **34** R45–R91
[7] Wehlitz R 2010 Simultaneous emission of multiple electrons from atoms and molecules using synchrotron radiation *Adv. At. Mol. Opt. Phys.* **58** 1–76
[8] Lablanquie P, Penent F and Hikosaka Y 2016 Multi-electron coincidence spectroscopy: double photoionization from molecular inner-shell orbitals *J. Phys. B: At. Mol. Opt.* **49** 182002
[9] Schippers S, Perry-Sassmannshausen A, Buhr T, Martins M, Fritzsche S and Müller A 2020 Multiple photodetachment of atomic anions via single and double core-hole creation *J. Phys. B: At. Mol. Opt.* **53** 192001
[10] Allaria E *et al* 2012 Highly coherent and stable pulses from the FERMI seeded free-electron laser in the extreme ultraviolet *Nat. Photon.* **6** 699–704
[11] Ackermann W *et al* 2007 Operation of a free-electron laser from the extreme ultraviolet to the water window *Nat. Photon.* **1** 336–42
[12] Emma P *et al* 2010 First lasing and operation of an ångstrom-wavelength free-electron laser *Nat. Photon.* **4** 641–7
[13] Ishikawa T *et al* 2012 A compact x-ray free-electron laser emitting in the sub-ångström region *Nat. Photon.* **6** 540–4
[14] Kang H S *et al* 2017 Hard x-ray free-electron laser with femtosecond-scale timing jitter *Nat. Photon.* **11** 708–13
[15] Prat E *et al* 2020 A compact and cost-effective hard x-ray free-electron laser driven by a high-brightness and low-energy electron beam *Nat. Photon.* **14** 748–54
[16] Decking W *et al* 2020 A MHz-repetition-rate hard x-ray free-electron laser driven by a superconducting linear accelerator *Nat. Photon.* **14** 391–7
[17] Bilderback D H, Elleaume P and Weckert E 2005 Review of third and next generation synchrotron light sources *J. Phys. B: At. Mol. Opt.* **38** S773
[18] Berrah N *et al* 2010 Non-linear processes in the interaction of atoms and molecules with intense EUV and x-ray fields from SASE free electron lasers (FELs) *J. Mod. Opt.* **57** 1015–40
[19] Duris J *et al* 2019 Tunable isolated attosecond x-ray pulses with gigawatt peak power from a free-electron laser *Nat. Photon.* **14** 30–36
[20] Li S *et al* 2022 Attosecond coherent electron motion in Auger-Meitner decay *Science* **375** 285–90
[21] Canton S E *et al* 2015 Visualizing the non-equilibrium dynamics of photoinduced intramolecular electron transfer with femtosecond x-ray pulses *Nat. Commun.* **6** 6359
[22] Glownia J M *et al* 2016 Self-referenced coherent diffraction x-ray movie of ångstrom- and femtosecond-scale atomic motion *Phys. Rev. Lett.* **117** 153003
[23] Varvarezos L *et al* 2023 Controlling fragmentation of the acetylene cation in the vacuum ultraviolet via transient molecular alignment *J. Phys. Chem. Lett.* **14** 24–31

[24] Wabnitz H, De Castro A R B, Gürtler P, Laarmann T, Laasch W, Schulz J and Möller T 2005 Multiple ionization of rare gas atoms irradiated with intense VUV radiation *Phys. Rev. Lett.* **94** 023001
[25] Sorokin A A, Wellhöfer M, Bobashev S V, Tiedtke K and Richter M 2007 X-ray-laser interaction with matter and the role of multiphoton ionization: free-electron-laser studies on neon and helium *Phys. Rev.* A **75** 051402
[26] Moshammer R *et al* 2007 Few-photon multiple ionization of Ne and Ar by strong free-electron-laser pulses *Phys. Rev. Lett.* **98** 203001
[27] Sorokin A A, Bobashev S V, Feigl T, Tiedtke K, Wabnitz H and Richter M 2007 Photoelectric effect at ultrahigh intensities *Phys. Rev. Lett.* **99** 213002
[28] Richter M, Amusia M Y, Bobashev S V, Feigl T, Juranić P N, Martins M, Sorokin A A and Tiedtke K 2009 Extreme ultraviolet laser excites atomic giant resonance *Phys. Rev. Lett.* **102** 163002
[29] Hoener M *et al* 2010 Ultraintense x-ray induced ionization, dissociation, and frustrated absorption in molecular nitrogen *Phys. Rev. Lett.* **104** 253002
[30] Motomura K *et al* 2009 Multiple ionization of atomic argon irradiated by EUV free-electron laser pulses at 62 nm: evidence of sequential electron strip *J. Phys. B: At. Mol. Opt.* **42** 221003
[31] Schmid G *et al* 2019 Tracing charge transfer in argon dimers by XUV-pump IR-probe experiments at FLASH *J. Chem. Phys.* **151** 84314
[32] Düsterer S *et al* 2019 Two-color XUV+NIR femtosecond photoionization of neon in the near-threshold region *New J. Phys.* **21** 063034
[33] Richardson V *et al* 2010 Two-photon inner-shell ionization in the extreme ultraviolet *Phys. Rev. Lett.* **105** 013001
[34] Hadjipittas A, Banks H I B, Bergues B and Emmanouilidou A 2020 Sequential single-photon and direct two-photon absorption processes for Xe interacting with attosecond XUV pulses *Phys. Rev.* A **102** 043108
[35] Kastirke G *et al* 2020 Double core-hole generation in O_2 molecules using an x-ray free-electron laser: molecular-frame photoelectron angular distributions *Phys. Rev. Lett.* **125** 163201
[36] Fouda A E A, Koulentianos D, Young L, Doumy G and Ho P J 2022 Resonant double-core excitations with ultrafast, intense x-ray pulses *Mol. Phys.* **121** e2133749
[37] Mazza T *et al* 2020 Mapping resonance structures in transient core-ionized atoms *Phys. Rev.* X **10** 041056
[38] Young L *et al* 2010 Femtosecond electronic response of atoms to ultra-intense x-rays *Nature* **466** 56–61
[39] Braune M *et al* 2015 Electron angular distributions of noble gases in sequential two-photon double ionization *J. Mod. Opt.* **63** 324–33
[40] Varvarezos L *et al* 2021 Near-threshold two-photon double ionization of Kr in the vacuum ultraviolet *Phys. Rev.* A **103** 022832
[41] Carpeggiani P A *et al* 2018 Complete reconstruction of bound and unbound electronic wavefunctions in two-photon double ionization *Nat. Phys.* **15** 170–7
[42] Rouzée A *et al* 2011 Angle-resolved photoelectron spectroscopy of sequential three-photon triple ionization of neon at 90.5 eV photon energy *Phys. Rev.* A **83** 031401
[43] Radcliffe P *et al* 2012 Atomic photoionization in combined intense XUV free-electron and infrared laser fields *New J. Phys.* **14** 043008
[44] Mazza T *et al* 2016 Angular distribution and circular dichroism in the two-colour XUV+NIR above-threshold ionization of helium *J. Mod. Opt.* **63** 367–82
[45] Fukuzawa H and Ueda K 2020 X-ray induced ultrafast dynamics in atoms, molecules, and clusters: experimental studies at an x-ray free-electron laser facility SACLA and modelling *Adv. Phys.* X **5** 1785327
[46] Bostedt C *et al* 2013 Ultra-fast and ultra-intense x-ray sciences: first results from the Linac coherent light source free-electron laser *J. Phys. B: At. Mol. Opt.* **46** 164003
[47] Costello J, Kennedy E and Nikolopoulos L 2016 Short wavelength free electron lasers *J. Mod. Opt.* **63** 285–7
[48] Ueda K 2021 Science at x-ray free electron lasers *Appl. Sci.* **11** 10622
[49] Huang N, Deng H, Liu B, Wang D and Zhao Z 2021 Features and futures of x-ray free-electron lasers *Innovation* **2** 100097
[50] Seddon E A *et al* 2017 Short-wavelength free-electron laser sources and science: a review* *Rep. Prog. Phys.* **80** 115901
[51] Rossbach J, Schneider J R and Wurth W 2019 10 years of pioneering x-ray science at the free-electron laser FLASH at DESY *Phys. Rep.* **808** 1–74
[52] Feldhaus J, Krikunova M, Meyer M, Möller T, Moshammer R, Rudenko A, Tschentscher T and Ullrich J 2013 AMO science at the FLASH and European XFEL free-electron laser facilities *J. Phys. B: At. Mol. Opt.* **46** 164002
[53] Meyer M, Costello J T, Düsterer S, Li W B and Radcliffe P 2010 Two-colour experiments in the gas phase *J. Phys. B: At. Mol. Opt.* **43** 194006
[54] Orfanos I *et al* 2022 Two-XUV-photon double ionization of neon *Phys. Rev.* A **106** 043117
[55] Katravulapally T and Nikolopoulos L A A 2020 Perturbative theory of statistically averaged atomic dynamics in fluctuating laser fields *Phys. Rev.* A **102** 053111
[56] Richter M *et al* 2003 Measurement of gigawatt radiation pulses from a vacuum and extreme ultraviolet free-electron laser *Appl. Phys. Lett.* **83** 2970–2
[57] Feigl T, Yulin S, Benoit N and Kaiser N 2006 EUV multilayer optics *Microelectron. Eng.* **83** 703–6
[58] Radcliffe P *et al* 2007 An experiment for two-color photoionization using high intensity extreme-UV free electron and near-IR laser pulses *Nucl. Instrum. Methods Phys. Res.* **583** 516–25
[59] Eland J H D, Vieuxmaire O, Kinugawa T, Lablanquie P, Hall R I and Penent F 2003 Complete two-electron spectra in double photoionization: the rare gases Ar, Kr, and Xe *Phys. Rev. Lett.* **90** 053003
[60] Richardson V 2011 *Two Photon and Two Colour Ionisation of Atoms in Intense Extreme-UV and Optical Laser Fields* (Dublin City University)
[61] Wuilleumier F and Krause M O 1974 Photoionization of neon between 100 and 2000 eV: single and multiple processes, angular distributions, and subshell cross sections *Phys. Rev.* A **10** 242–58
[62] Kikas A, Osborne S J, Ausmees A, Svensson S, Sairanen O P and Aksela S 1996 High-resolution study of the correlation satellites in photoelectron spectra of the rare gases *J. Electron Spectrosc. Relat. Phenom.* **77** 241–66
[63] Haar D 1961 Ter theory and applications of the density matrix *Rep. Prog. Phys.* **24** 307
[64] Bermúdez Macias I J, Düsterer S, Ivanov R, Liu J, Brenner G, Rönsch-Schulenburg J, Czwalinna M K and Yurkov M V 2021 Study of temporal, spectral, arrival time and energy fluctuations of SASE FEL pulses *Opt. Express* **29** 10491

[65] Saldin E L, Schneidmiller E A and Yurkov M V 1999 FAST: a three-dimensional time-dependent FEL simulation code *Nucl. Instrum. Methods Phys. Res.* A **429** 233–7
[66] Kramida A, Ralchenko Y and Reader J NIST atomic spectra database Available online (available at: https://physics.nist.gov/asd)
[67] Uiterwaal C J G J, Gebhardt C R, Schröder H and Kompa K-L 2004 Predicting intense-field photoionization of atoms and molecules from their linear photoabsorption spectra in the ionization continuum *Eur. Phys. J.* D **30** 379–92
[68] Lambropoulos P 1980 Reaching VUV transitions with multiphoton processes *Appl. Opt.* **19** 3926–33
[69] Hitchcock A P and Brion C E 1980 Neon K-shell excitation studied by electron energy-loss spectroscopy *J. Phys. B: At. Mol. Opt.* **13** 3269–73